8

Thermal Conductivity Enhancement of PCM using Exfoliated Graphite

8.1 INTRODUCTION

Thermal energy storage systems play a critical role in storing thermal energy to fulfill the gap between demand and supply and in situations, where it is essential to store surplus energy that would have else been wasted. An efficient TESS (thermal Energy Storage System) not only improves the reliability and performance of thermal energy systems but also helps in conserving energy. Thus, the development of TESS is a key issue in realizing the efficient utilization of renewable energy. Numerous phase change materials (PCMs) are developed for thermal energy storage applications and becoming more and more attractive due to their several benefits as discussed in section 1.1. However, most of the PCMs suffer with low thermal conductivity (0.2 W m^{-1} K^{-1} to 1.0 W m^{-1} K^{-1}) [Cabeza et al., 2002; Yuping and Wang, 2015]. The intrinsic poor thermal conductivity impedes the process of effective heat transfer in PCM based TESS by extending the charging (heat storage) and discharging (heat removal) periods [Mills et al., 2006, Mehling et al., 2008]. This also degrades the TESS performance to a large extent. This compels to tailor the thermal conductivity of PCMs for superior LHTESS performance. Substantial efforts are made by researchers to overcome the issue of poor thermal conductivity of PCMs. Some of the important methodologies developed/adopted are (i) deployment of extended surface/fins (ii) imbedding PCM into thermally conductive matrix/foam, (iii) encapsulation of PCM, and (iv) mixing of nanoparticles with PCM. Among these methodologies, exfoliated graphite composite based PCM are popular, where exfoliated graphite (ExG) can absorb large amount of PCM by capillary action and provide a continuous graphitic network, leading to the enhanced thermal conductivity of PCM.

Sari and Karaipekli, 2007 explored the effect of ExG on a paraffin based PCM thermal conductivity. The PCM-ExG composite with 10 wt% ExG was found most encouraging one for TES applications because of its good thermal conductivity and form-stability. Wang et al., 2009, mentioned that thermal conductivity of PEG-EG composites (large latent heat ~ 161.2 kJ kg^{-1}) increased about four times with 10 wt% of ExG as compared to pure PEG. Zhog et al., 2010 studied the effects of different densities of ExG matrices on paraffin-based LHTES performance. The linear relation between bulk ExG density and thermal conductivity was observed. Duan et al., 2014 prepared $CaCl_2 \cdot 6H_2O$-ExG composite (PCM) by vacuum impregnation process. They observed that the thermal conductivity of PCM composites improved from 0.596 W m^{-1} K^{-1} to 8.796 W m^{-1} K^{-1} which was about 14 times higher as compared to pure $CaCl_2 \cdot 6H_2O$. Lee et al., 2014, prepared erythritol-ExG composites and found that the thermal conductivity can be increased up to 3.56 W m^{-1} K^{-1}. Yuan et al. 2014 prepared PCM (eutectic of myristic acid, palmitic acid and stearic acid) -ExG composite with 13:1 mass ratio. Authors reported an enhancement in thermal conductivity of investigated PCM-ExG composites and also showed enhanced thermal stability upto 1000 heating and cooling cycles. Feng et al., 2015 conducted numerical and experimental studies on heat transfer properties of paraffin-ExG composite and showed the anisotropic thermal conductivity behavior in this system. Ling et al. 2015 investigated thermal behavior of RT44HC and ExG composites with different packing densities. They showed enhancement in thermal conductivity of composites with increasing packing

density. The composites thermal conductivity was more sensitive for packing density than mass fraction of ExG. WA et al., 2015, prepared hydrated salt- ExG composites using impregnation and coated it with paraffin. It was observed that phase segregation and supercooling were reduced in composites. Furthermore, thermal conductivity of the composites was enhanced up to 3.6 W m^{-1} K^{-1}. Zhong et al. 2015 prepared PCM-ExG composites comprising $LiNO_3$-NaCl, $LiNO_3$-KCl and $LiNO_3$-$NaNO_3$ eutectic molten salts PCMs by solution impregnation technique and investigated their thermal behaviors. These composites were found more homogeneous as compared to other salt-ExG composites, prepared using infiltration or compression methods. The thermal conductivity of eutectic salt mixtures was enhanced upto 7 times using ExG. Xiao et at., 2015 prepared $NaNO_3$ and KNO_3 eutectic PCM and PCM-ExG composites with different ExG weight fractions (5%, 10% and 20%) to improve the thermal conductivity of PCM composites. They measured thermal conductivity of eutectic PCM and PCM-ExG composites using steady state testing rig. The thermal conductivities of eutectic PCM were increased about two, three and seven times with 5 wt% , 10 wt% and 20 wt% ExG, respectively. Zhang et al., 2016 investigated effect of exfoliated graphite on heating and cooling time on capric acid, palmitic acid and stearic acid based ternary eutectic compositions. They reported that the melting and solidification time can be reduced significantly by using ExG. The PCM-ExG composites also exhibited good thermal stability for 500 heating and cooling cycles.

In this study, attempts are made to develop PCM-exfoliated graphite composites to enhance thermal properties of PCMs for low and high temperature thermal energy storage applications This includes: (i) optimization of exfoliation process of natural graphite flakes (NGF), (ii) development of PCM-ExG composites using low and high temperature phase change materials, (iii) investigation of PCM-ExG composites thermal conductivity with different ExG weight fractions and densities.

8.2 EXFOLIATION OF NATURAL GRAPHITE FLAKES

The graphite is made of graphene layers or two dimensional sheets made through sp2 hybridization of carbon atoms. The graphene layers are bonded by weak van Der Waals interaction and the spacing between two layers is 3.37 Å [Yasim et al., 2006]. The intercalating molecules can enter between these graphene layers through diffusion by edge planes because of weak Van Der Waals force [Xio et al., 2002]. The resultant product, composed of intercalant and graphite, is known as expandable graphite or graphite intercalation compounds (GICs) [Xio et al., 2002; Chen et a., 2003; Dreyer et al., 2010]. Daniel et al. [Dreyer et al., 2010], suggested that natural graphite flake (NGF) has composite structure and intrinsic localized defects in p-structure may provide seeding points for oxidation process. The nitric acid and potassium perchlorate are used as oxidative agents for better oxidation than using only single intercalating agent. The intercalation process increases the distance between graphite layers, for example the distance between pristine graphite layers is increased from 0.34 nm to 0.53nm with potassium-GIC [Okamoto et al., 2001]. Exfoliated graphite (ExG) refers to a defective graphite with large carbon layer separation as compared to that of bulk graphite. The process used to convert GIC into the exfoliated graphite (ExG) is termed exfoliation process and this may include mechanical, thermal and chemical means. [Panwar et al., 2009]. The exfoliation process explained schematically in Figure 8.1, showing bulk NGF in conjunction with GIC and ExG, sequentially.

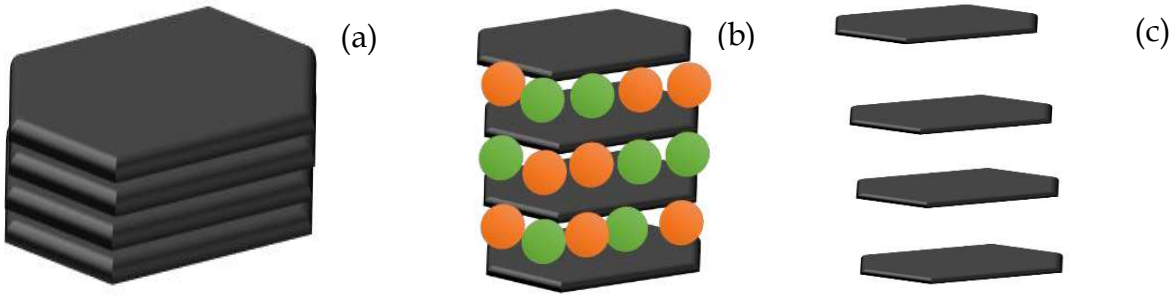

Figure 8.1: Schematic representation for (a) natural graphite flake, (b) graphite intercalation compounds, and (c) exfoliated graphite respectively.

Exfoliated graphite consists of highly micro porous structure and thus, large surface area. These large pores in ExG help to absorb large weight fraction of PCM and thus, assist in reducing the leakage of PCM in liquid state i.e. charged state. The ExG - PCM composite systems are cost effective also as the process avoids any encapsulation process, thus minimizing the overall cost of the system [Sari, 2004]. Therefore, PCM–ExG composite systems are of great potential for TES applications.

8.2.1 Experimental Details

8.2.1.1 Materials

The natural graphite flakes are purchased from Sigma Aldrich and used to develop exfoliation graphite. Sulfuric acid (99% pure), nitric acid (80% pure) and potassium permanganate (purity) are received from Fisher Scientific for chemical treatment of graphite flakes and to produce the exfoliated graphite.

8.2.1.2 Preparation of Intercalated Graphite Compound and Thermal Exfoliation

The chemical treatment process is adopted as explained schematically in Figure 8.2, showing the synthesis of graphite intercalation compounds from natural graphite flakes (NGFs).

In first step, NGFs are taken in a beaker (Figure 8.2(a)), then H_2SO_4, HNO_3 and $KMnO_4$ solution in 9:3:0.44 weight ratio is slowly added in 1 g NGFs (Figure 8.2(b)) [Zhang et al., 2010]. Afterward, the resultant mixture is continuously stirred for 3 hours using magnetic stirrer at ambient temperature, Figure 8.2(c). After three hours of continuous stirring, the chemically treated NGFs are rinsed several times using deionized (DI) water to achieve pH ~ 6-7, as shown in Figure 8.2(d). The chemically treated NGFs are dried in oven at ~ 110 ^{o}C for ~12 hrs. These dried chemically modified NGFs are termed as expandable graphite or GIC. The GICs are kept inside a box furnace for 50-60 seconds at 950-1000 ^{o}C to get the exfoliated graphite. This thermal shock assists graphite intercalation compounds conversion into exfoliated graphite. The optimized process led to ~ 250 times volume expansion, showing large surface area and porous structures.

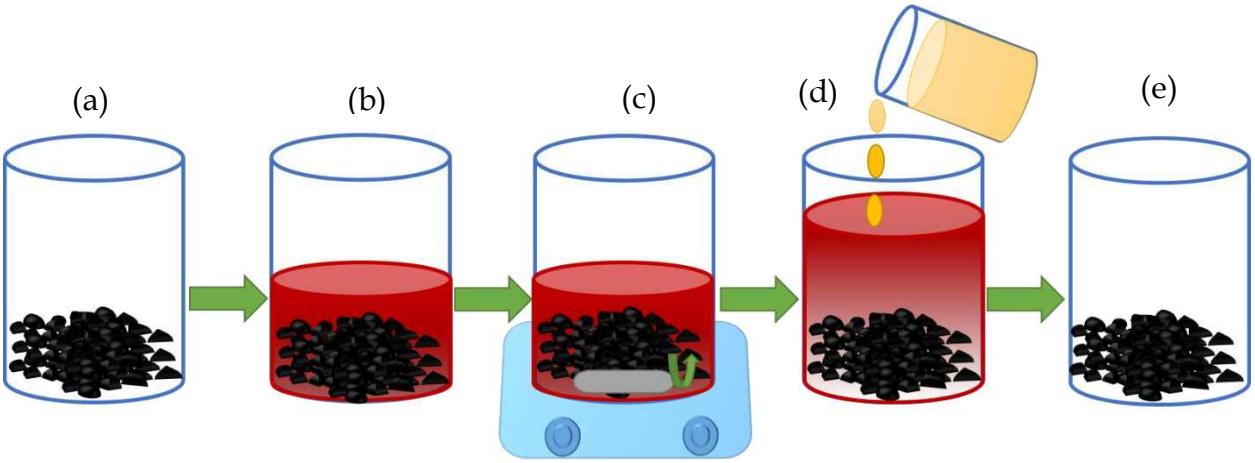

Figure 8.2: Schematic representation of process to get graphite intercalation compounds from natural graphite flakes. (a) natural graphite flakes (NGFs) in beaker, (b) adding H_2SO_4, HNO_3 and $KMnO_4$ solution in NGFs, (c) stirring of solution using magnetic stirrer for ~3 hours, (d) addition of DI water to reduce pH of chemically treated NGFs to 6-7 and (e) graphite intercalation compounds after

The whole graphite exfoliation process flow diagram is explained in Figure 8.3, with exfoliated graphite.

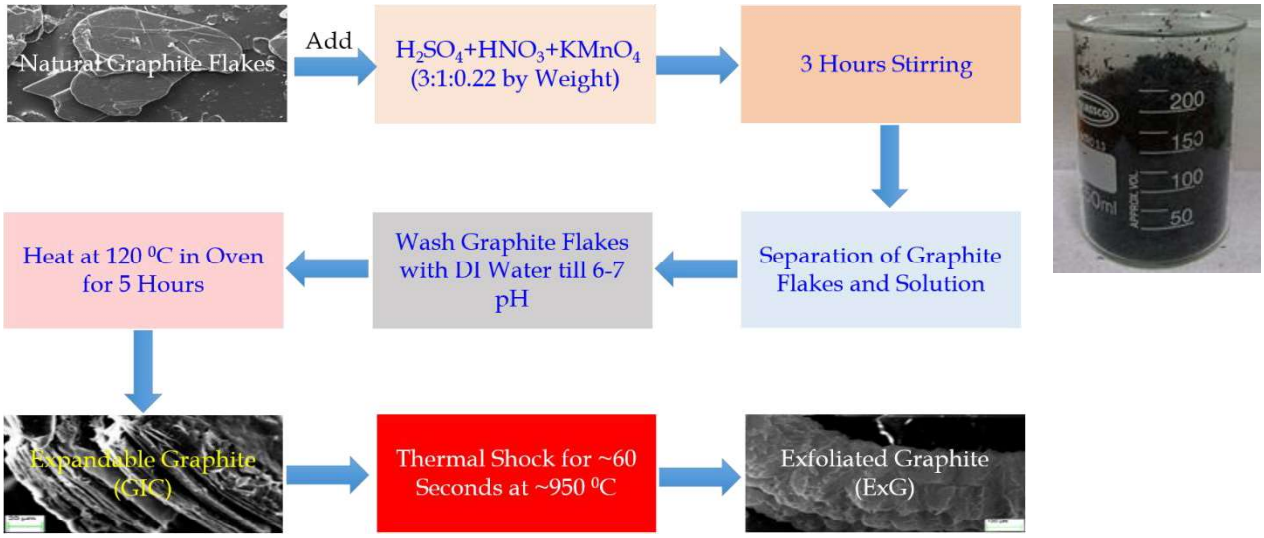

Figure 8.3: Flow diagram for the process of exfoliation of graphite from natural graphite flakes, with actual photograph of exfoliated graphite (right panel) in beaker

8.2.2 Results and Discussion

8.2.2.1 Scanning Electron Microscopic Analysis

The microstructural properties are investigated using SEM measurements for NGFs, GICs and ExG samples. The microscopic results are summarized in Figure 8.4. The compact edges of NGF, can be seen in Figure 8.4(a), opens up after chemical intercalation, as shown in Figure 8.4(b). This

edge opening supports the increase in interplaner graphite layers spacing along c-axis. The observed opening is attributed to the intercalation of sulfate and nitrate ions between NGFs basal layers along c-axis. The intercalates sandwiched between graphite layers, decompose during high temperature (950 ^{o}C) thermal shock, exerting outward force on graphite layers, leading to the wider separation among them. The graphite crystal structure deforms during this expansion process, showing large volume enhancement upto 250 times as compared to that of the original NGF sample. The wormlike structures, Figure 8.4 (c), are observed for exfoliated graphite samples. These wormlike structures with diamond shaped pores (Figure 8.4(c)) suggest the enhanced porosity in the final thermochemically treated ExG samples, where edges are connected through pores. Further, at higher magnification (Figure 8.4(d)) the exfoliated graphite looks like paper sheets, holding together at the boundaries via weak Van Der Waals interactions.

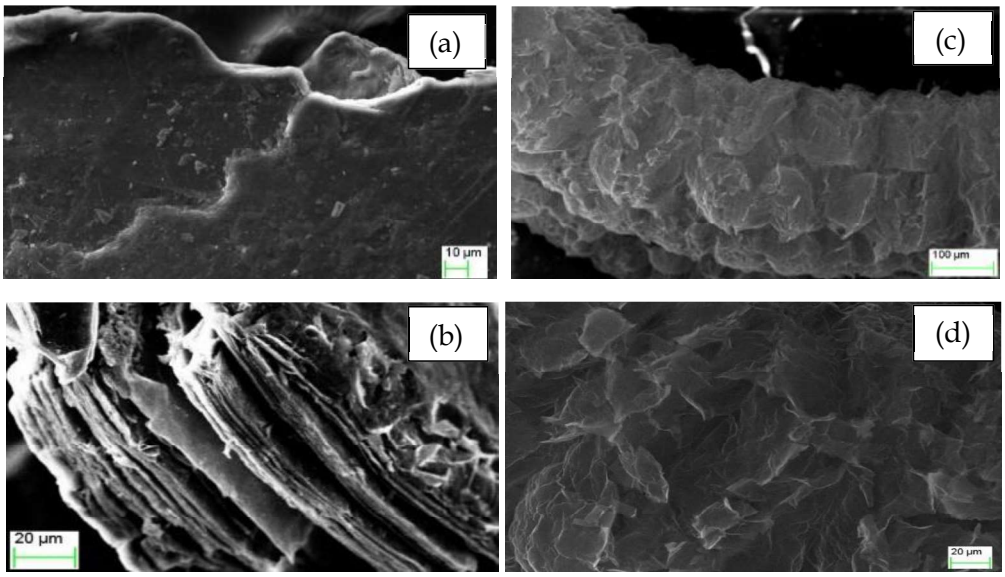

Figure 8.4: SEM micrographs for (a) NGFs (magnification 1kx), (b) GICs (magnification 1kx), (c) ExG (magnification 240x) and (d) ExG (magnification 1kx)

8.2.2.2 X-*ray* Diffraction Analysis

We carried out powder X-ray diffraction measurements to investigate the crystallinity of NGFs, GICs and ExG samples using Bruker D8 Advance X-ray diffractometer. The pXRD patterns were recorded in the range of 10° to 60° with 0.02° s^{-1} scanning rate. The representative pXRD diffractographs of NGFs, GICs and EXG are plotted in Figure 8.5 for 10 – 60^{o} 2Θ range. The diffraction peaks at 2Θ=26.5°, 25.7° and 26.5° confirm support the presence of carbon-carbon bond in graphite after intercalation and oxidation of NGFs [Mukhopadhyay and Gupta, 2013]. The intensity related to NGF, is relatively higher as compared to that of GICs and ExG samples. The broader full width half maximum (FWHM) and reduced intensity of GICs and ExG samples as compared to that of NGFs clarify that crystal imperfections are increased and crystallinity of CIG and ExG samples is reduced after intercalation and thermal exfoliation processes [Mukhopadhyay and Gupta, 2013].

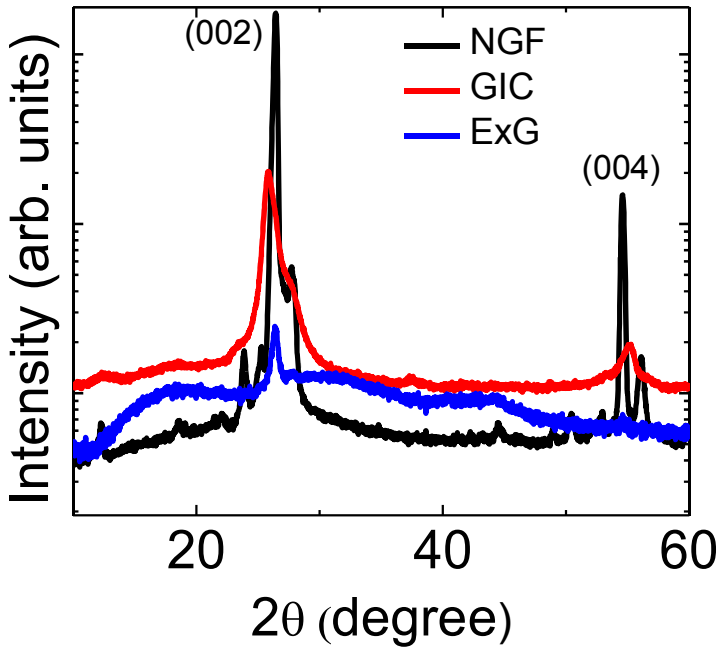

Figure 8.5: Powder X-Ray diffractographs of natural graphite flakes, graphite intercalation compounds and exfoliated graphite

8.2.2.3 Raman Spectroscopic Analysis

The room temperature Raman spectroscopic measurements were carried out to confirm the formation of nanostructured graphene like structures after exfoliation and results are plotted in Figure 8.6. The NGFs, GICs and ExG Raman spectrographs can be easily distinguished from each other. The sharp G band peak, a weaker D band peak in conjunction with a 2D band resonance peak specifies the existence of graphene like structures in ExG samples.

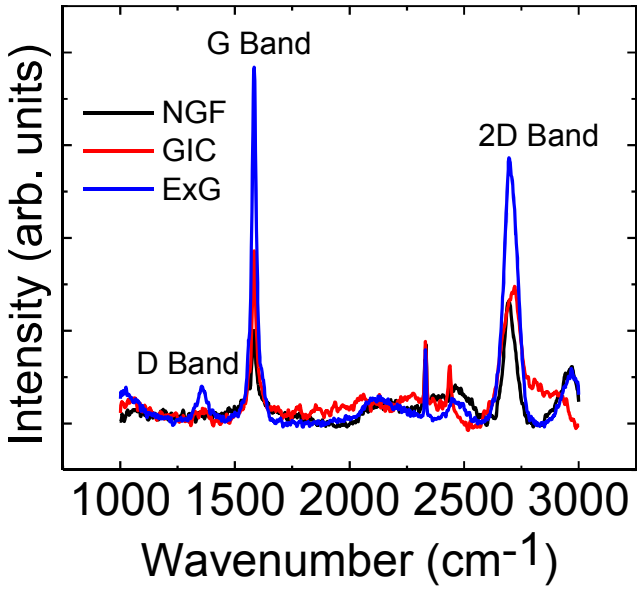

Figure 8.6: Raman spectrograph of natural graphite flakes, graphite intercalation compound and exfoliated graphite

The origin of D band in graphitic system is attributed to the lattice defects and disorders and is observed at ~ 1355 cm^{-1} [Mukhopadhyay and Gupta, 2013]. The absence of this peak in NGFs and CIG suggests that these systems are relatively less distorted as compared to that of ExG samples. The presence of stronger G peak, at 1580 cm^{-1} in ExG sample, substantiates the sp^2 bonded carbon and thus, the formation of graphene like structures in ExG sample [Mukhopadhyay and Gupta, 2013]. The second order 2D resonance band at ~ 2700 cm^{-1} can be observed in all these samples, yet the relative intensity of this vibrational band is the highest for ExG and the lowest for NGFs samples. This broad peak around ~2700 cm^{-1} (2D) is attributed to multi-layered graphene like structure. This again supports the formation of nanostructured graphene like structures in ExG samples. The very low intensity of D/G ratios (~0.09) supports the presence of well-ordered graphene crystals in ExG samples. The weak vibrational modes around ~ 2330 and 2435 cm^{-1} are attributed to intercalants in ICG and ExG samples.

8.3 ORGANIC PCM-EXFOLIATED GRAPHITE COMPOSITES

8.3.1 Preparation of Myristic Acid-ExG Composites

Myristic acid (MA) purchased form Alfa Aesar, was mechanically mixed with thermochemically synthesized ExG using a vertical mixing arrangement, as shown in Figure 8.7 (a). MA was mixed in liquid phase by maintaining the base platform at ~75 ^{0}C temperature while mixing. The mechanical mixing assisted the uniform impregnation of MA into the porous exfoliated graphite matrix and to realize the shape stabilized MA-ExG composites with high thermal conductivity. The MA-ExG composite matrix were prepared using 5, 10 and 15 weight percentage of ExG to understand the effect of ExG on thermal conductivity and heat release process.

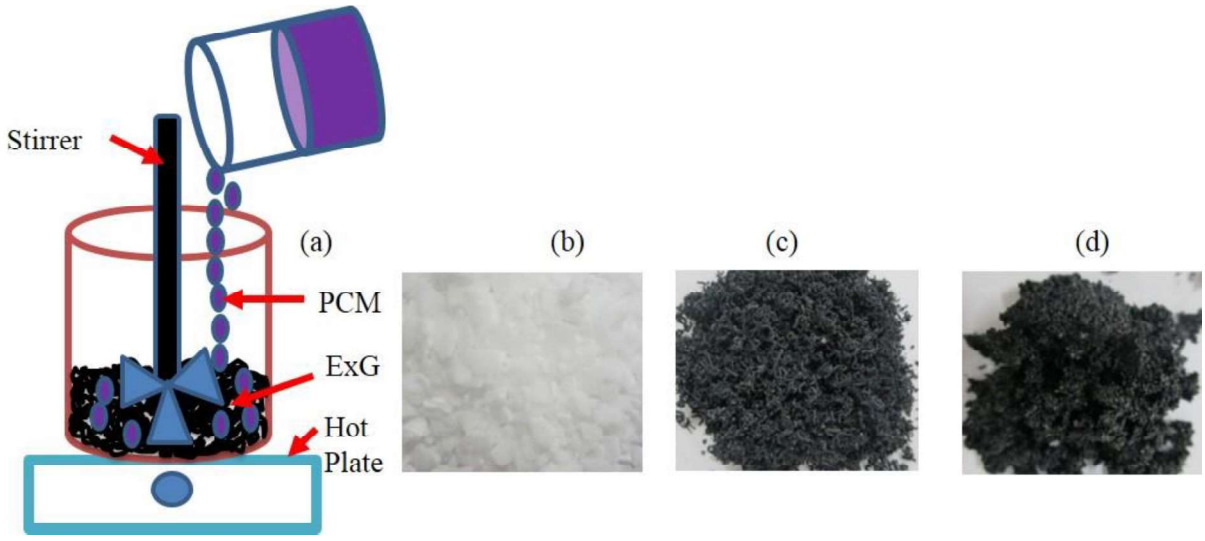

Figure 8.7: (a) Schematic of set up for preparation of MA-ExG composite, (b) photograph of pristine MA, (c) photograph of ExG and (d) photograph of MA-ExG composite

The large porosity of ExG assisted the large fraction of myristic acid impregnation inside the ExG pores, where capillary forces between liquid MA and pores in ExG helped to provide the stable leak free compact shaped composite systems [Mehling and Cabeza 2008]. The unmagnified

photographs are shown in Figure 8.7 (b, c and d) for pristine MA, ExG and MA-ExG, with 10% ExG by weight composite systems, respectively. The ExG-MA composite photograph, Figure 8.7 (d), suggests that MA is trapped inside the pores even in liquid state. Thus, ExG may also overcome of the problem of PCM leakage during thermal charging and discharging of PCM in conjunction with enhanced thermal conductivity.

8.3.2 Results and Discussion

8.3.2.1 Scanning Electron Microscopic Analysis

We carried out microstructural investigations of MA-ExG composite samples to understand the mechanism of PCM impregnation inside the ExG pores using Scanning Electron Microscope. The respective SEM micrographs are shown in Figure 8.8 for MA-ExG composite sample. The SEM micrograph supports the hypothesis of impregnating MA inside ExG pores. The swelled region is attributed to the MA inside ExG pores, as shown in Figure 8.8 (a). The SEM micrograph at higher resolution (2.8 k x), Figure 6.8 (b) represents that the MA has been impregnated inside the pores of the exfoliated graphite.

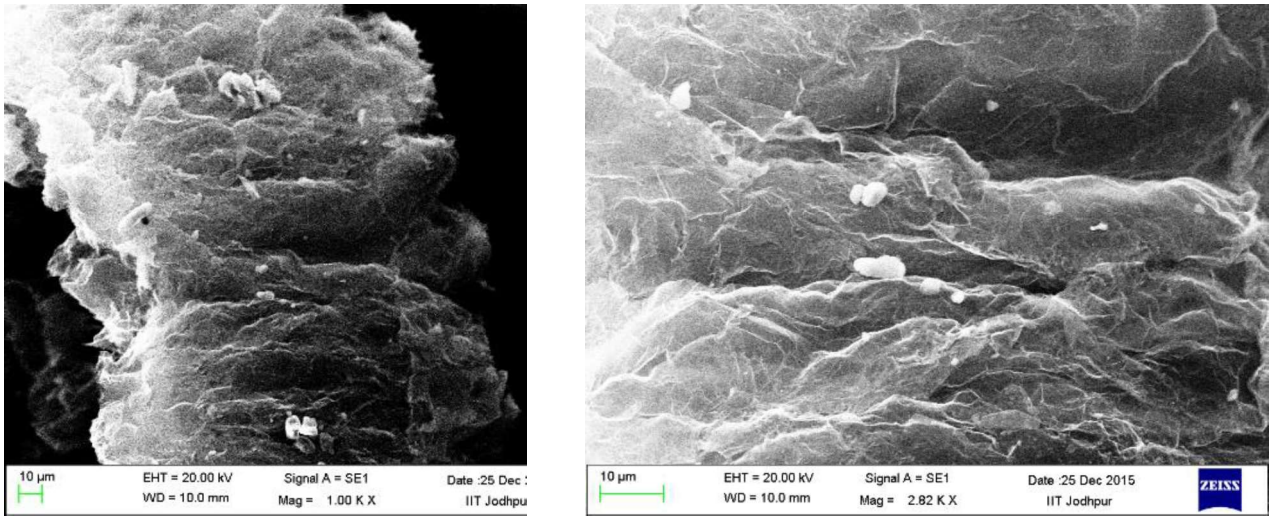

(a) (b)

Figure 8.8: SEM micrograph of MA-Exg (a) at 1k X, and (b) at 2.82k X

8.3.2.2 Fourier Transform Infrared Spectroscopic Analysis

We also carried out FTIR spectroscopic measurements on these samples to understand the chemical interaction between ExG and myristic acid in composite samples. The room temperature FTIR measurements are plotted in Figure 8.9 including myristic acid and different weight percent ExG derived MA-ExG composite samples.

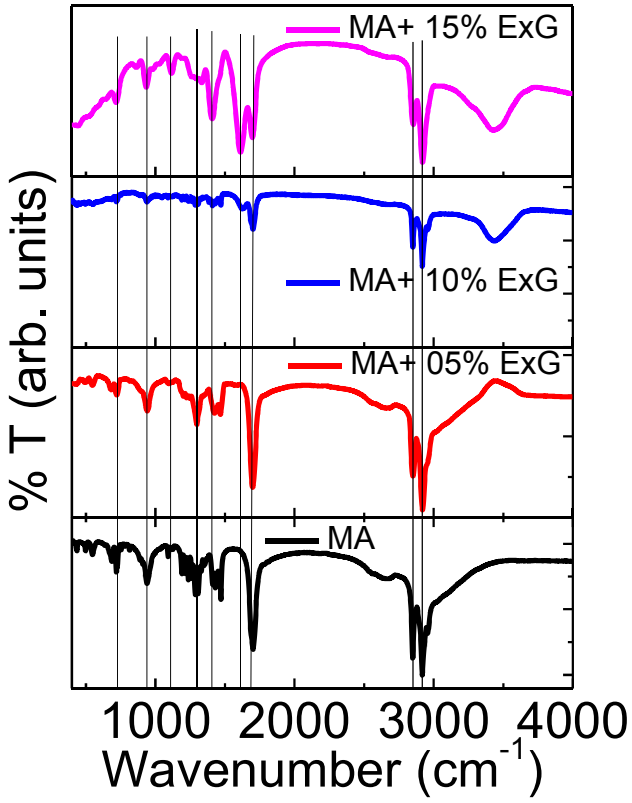

Figure 8.9: FTIR spectra of MA and MA-ExG composites with 5, 10 and 15 weight percentage of ExG

The chemical formula of myristic acid is $CH_3(CH_2)_{12}COOH$, which consists of C-H symmetric and asymmetric vibrations modes at 2910 and 2850 cm^{-1} respectively. MA also includes C=O stretching vibrations at 1700 cm^{-1} and out of plane and in plane swing vibrations of -OH functional group at 935 and 720 cm^{-1} respectively. All these vibrational modes are observed in the measured FTIR spectrum of myristic acid and different weight percent ExG-MA composite samples, as shown in Figure 8.9. C-H symmetric and asymmetric vibrational modes are unaffected in MA-ExG composite systems, suggesting that C-H bonds are not participating in bonding between ExG and MA. In contrast the vibration mode at 1700 cm^{-1}, representing C=O stretching mode showed significant changes after adding ExG in MA. The relative intensity of this mode is nearly unaffected in 5% ExG-MA sample, whereas drastically reduces for higher weight fraction of ExG in MA-ExG composite samples. This may be due to the partial bonding of MA in ExG-MA composites, where C-C bonds in ExG are getting attached with C=O bonds of MA. The vibrational modes at ~ 1300 and 1410 cm^{-1} are associated with C-C vibrational modes in ExG. These vibrational studies suggest that MA-ExG composites are physically bonded due to the capillary forces between ExG pores and MA and not chemically associated with each other. The strong physical bonding provides mechanical strength to hold the MA phase change material in ExG pores even in melting conditions of MA, avoiding any leakage in case of 10 and 15% ExG by weight in ExG-MA composite systems.

8.3.2.3 Thermal Conductivity Analysis

The thermal conductivity of PCM is an important parameter for thermal energy storage applications and that's why the thermal conductivity of pristine MA and MA-ExG composite samples are investigated using Hot Disk AB, Sweden make TPS 2500S thermal constant analyzer system. Thermal conductivity of MA and MA-ExG composites are measured using Ni sensor 5710 supplied with instrument. The sample pallets for measuring thermal conductivity of MA-ExG

composites are prepared using a dye, made of transparent acrylic material, and a pressing machine, shown in Figure 8.10 (a & b). The transparent dye is used to visualize and monitor the compression of PCM-ExG composite samples. The photographs of prepared MA-ExG pellets are shown in Figure 8.10 (c).

(a) (b) (c)

Figure 8.10: Real photographs of (a) transparent dye, (b) compression machine and (c) pallets of MA-ExG composite sample with 5, 10 and 15 weight fraction of ExG

The TPS sensor was sandwiched between two identical pallets to measure thermal conductivity of samples under investigation, shown in Figure 8.11(a & b). The detailed measurement procedure for measuring thermal conductivity of samples is explained in Chapter 3 and Kumar et al., 2017.

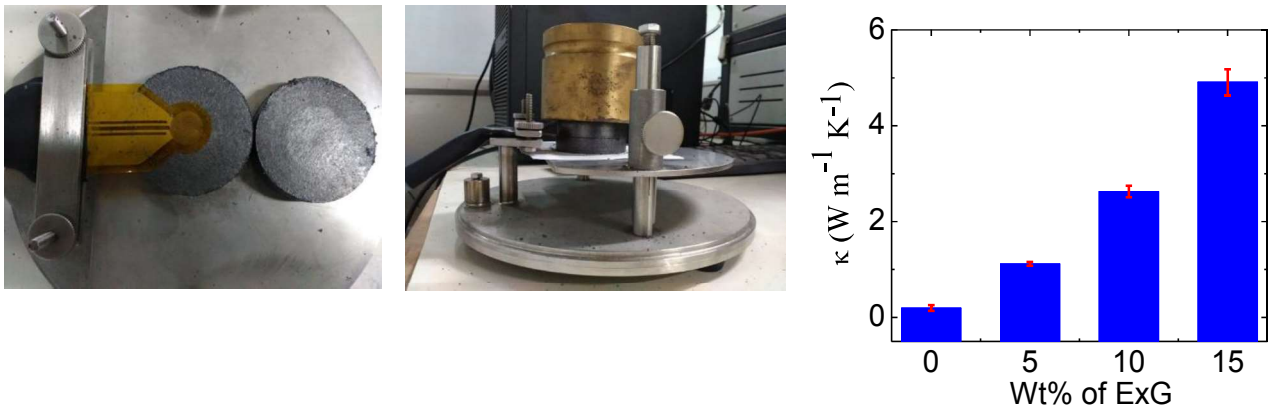

(a) (b) (c)

Figure 8.11: Measurement of thermal conductivity of MA-graphite composite samples, (a) Sensor for measuring thermal conductivity, (b) placement of sensor between two identical samples, (c) Average thermal conductivity of MA/ExG with 0, 5, 10 and 15 wt% of ExG

8.3.2.4 Temperature-History Analysis

In order to understand the effect of ExG in charging and discharging time of PCM, T-History measurements are carried out for pristine MA and ExG-MA composite samples using in-house developed T-history measuring set-up. The weight of the samples was kept constant ~20 g and filled in 20 mm diameter and 150 mm length glass tube. The samples were heated up to 75 °C in a heating chamber, ensuring MA is completely charged and is in liquid state. The cooling response i.e. temperature of samples as a function of time, was recorded at the time interval of every 10 seconds, in conjunction with chamber temperature, which was set at 30 °C during cooling. The measured temperature versus time response for pristine MA and 5, 10 and 15% ExG by weight MA-ExG samples are plotted in Figure 8.12(a).

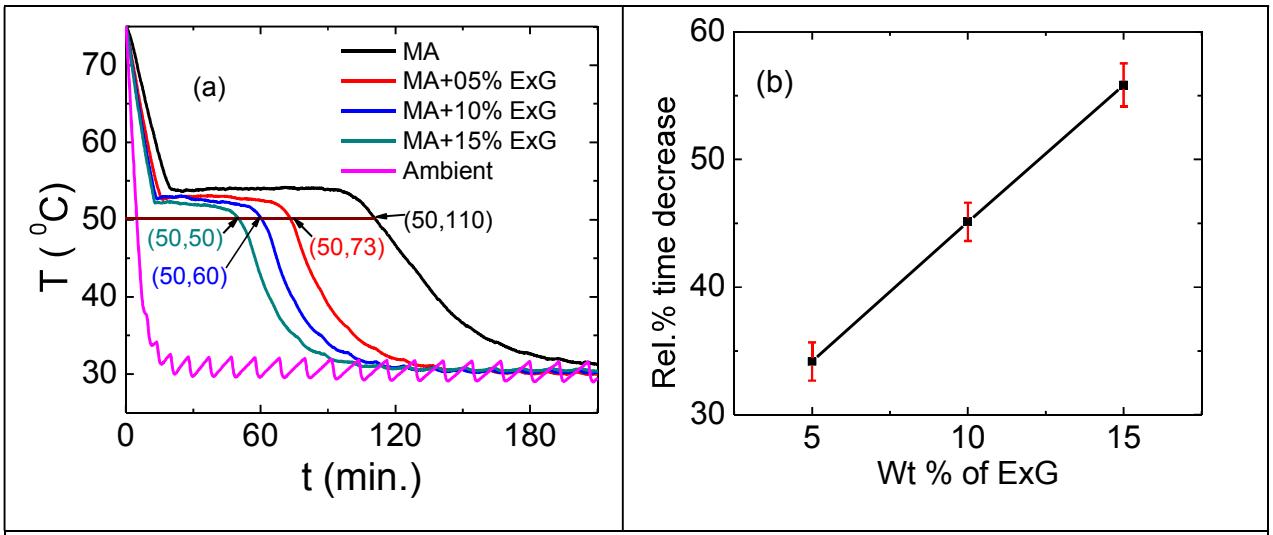

Figure 8.12: (a) Cooling response of Pristine MA, MA+5% ExG, MA+10% ExG and MA+15% ExG and (b) reduction in heat release time from 70-50 °C for , MA+5% ExG, MA+10% ExG and MA+15% ExG

We observed that pristine MA and 5, 10, and 15% ExG by weight ExG-MA samples took 110, 73, 60 and 50 minutes to cool from 70 °C to 50 °C respectively. These measurements explain the reduction in heat release time for ExG-MA composite samples as compared to the MA sample. The reduction in heat release time as a function of ExG weight fraction is plotted in Figure 8.12(b), suggesting that 15% ExG by weight-MA composite sample took ~ 55% less time as compared to the pure MA sample. This is because of thermally conducting ExG network in ExG-MA composite samples, providing continuous network for thermal transport across the graphitic basal planes.

8.4 INORGANIC HIGH TEMPERATURE PCM-EXFOLIATED GRAPHITE COMPOSITES

8.4.1 Experimental

8.4.1.1 Materials

The KNO_3 (purity 99%), HNO_3 (purity 99%), $LiNO_3$ (purity 99%) and NaCl (purity 99%) were purchased from Alfa Aesar and used to prepare eutectic of these materials.

8.4.1.2 Preparation of High Temperature Eutectic PCMs

The melting temperatures of $NaNO_3$, KNO_3, $LiNO_3$ and NaCl salts are very high and pose difficulties in handling and preparing homogeneous eutectic compositions of these salts. Hence, an indirect method is innovated to prepare the eutectic composition. This process assisted in preparing homogeneous mixture of these salts at normal room temperate (25 ^oC). Initially all salts were heated at 140 ^oC for one hour to evaporate any moisture content in the salt samples. After cooling down these samples to room temperatures under normal conditions, the samples were weighed in specific mass fraction ratio as tabulated in Table 8.1

Table 8.1: Compositions of salt eutectics made from $NaNO_3$, KNO_3, $LiNO_3$ and NaCl

S. NO.	Samples	Compositions (mass fraction ratio)
1	$NaNO_3$-KNO_3	50:50
2	$LiNO_3$-$NaNO_3$	54.8:45.2
3	$LiNO_3$-$NaNO_3$	48.8:51.2
4	$LiNO_3$-NaCl	88.8:11.2

Now the deionized water was added to the salt mixtures and stirred using magnetic stirrer for 30 minutes to dissolve completely and prepare homogeneous aqueous solution of respective salts. Thereafter, these aqueous salt samples were heated at 120 ^oC for 8 hours in laboratory oven and completely dried composite salt samples were collected. The prepared eutectic mixtures were used for further investigations

8.4.1.3 Preparation of PCM-ExG Composites

30g $LiNO_3$ –NaCl eutectic mixture was dissolved in 30ml deionized water. Further $LiNO_3$-Nacl/ExG composites were prepared by impregnating this eutectic solution using physical mixing method as explained in section 8.3.1.1. The mass fraction of ExG was varied as 5%, 10%, 15% and 20% weight percent, the pictures of prepared PCM-ExG composites are shown in Figure 8.13

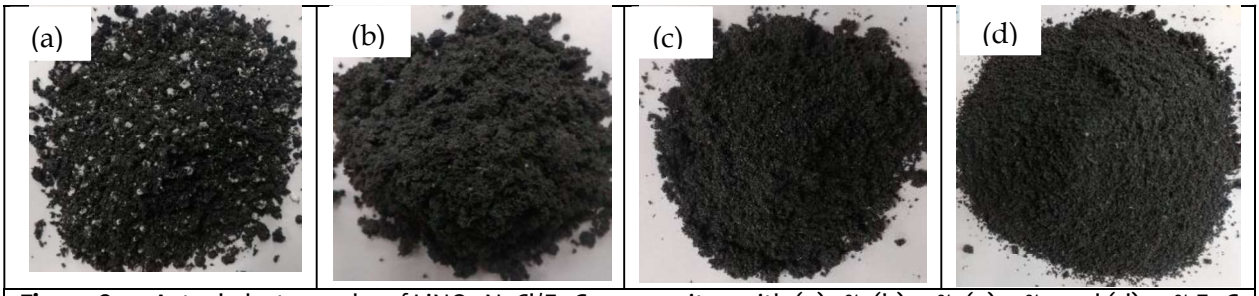

Figure 8.13: Actual photographs of $LiNO_3$-NaCl/ExG composites with (a) 5%, (b) 10%, (c) 15%, and (d) 20% ExG

Figure 8.13 indicates that composite with 5wt% ExG does not absorb eutectic PCM completely, whereas 10% ExG was sufficient to absorb the eutectic PCM completely.

8.4.2 Results and Discussion

8.4.2.1 Differential Scanning Calorimetric Analysis

The DSC measurements were carried out for the prepared salt eutectics as per procedure explained in section 4.4.2.2. The collected DSC thermographs are shown in Figure 8.14 and used to evaluate the respective thermal properties.

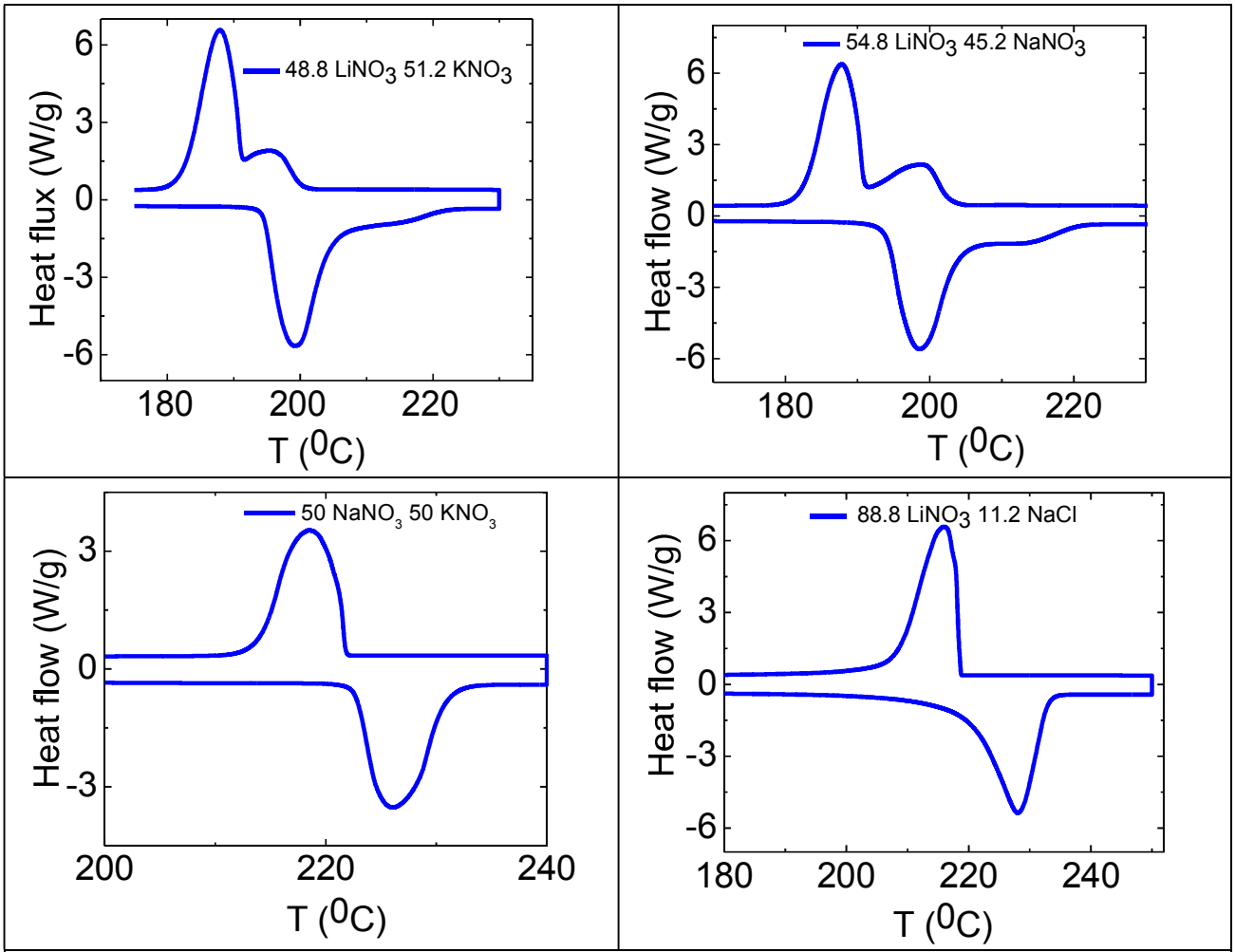

Figure 8.14: Differential scanning calorimetric thermographs for salt eutectics, (a) 54.8% $LiNO_3$ - 45.2%$NaNO_3$, (b) 48.8% $LiNO_3$ – 51.22%$NaNO_3$(b) (c) 50% $NaNO_3$ – 50% KNO_3, and (d) 88.8% $LiNO_3$ – 11.2% NaCl

The measured melting point and latent heat of fusion of synthesized high temperature PCMs are tabulated in Table 8.2.

Table 8.2: Melting point and latent heat of fusion of salt eutectics measured by DSC

S. No.	Samples with compositions in wt%	Melting point (°C)	Latent heat of fusion (kJ/kg)
1	50% $NaNO_3$- 50% KNO_3	225.8	107
2	54.8% $LiNO_3$ – 45.2% $NaNO_3$	198.62	258.2
3	48.8% $LiNO_3$- 25.8% $NaNO_3$	198.2	245.3
4	88.8% $LiNO_3$- 11.2% NaCl	228.8	302.5

The measured melting point and latent heat of fusion values are in good agreement with reported literature values [Zhou and Eames, 2016 and 2017].

8.4.2.2 Thermal Conductivity Analysis

Since the PCM-ExG composite particles are loosely connected together under normal conditions (Figure 18.13), the thermal conductivity and apparent density of PCM-ExG composites are low due to trapping of air between PCM-ExG composites and non-connectivity of graphite matrix. The low density of PCM is disadvantageous for latent heat thermal energy storage applications due to low thermal energy storage density and high cost for storage vessel. To understand the effect of different wt% of ExG and density of PCM-ExG composites, the thermal conductivity of $LiNO_3$-NaCl /ExG composite materials are measured for 10, 15 and 20 wt% ExG at 520, 620, 860, 1000, and 1400 kg m^{-3} densities. Density of $LiNO_3$-NaCl/ExG composites more than 14000 kg m-3 is not possible due to leakage of liquid PCM from graphite matrix. The $LiNO_3$-NaCl/ExG composite samples of 50 mm diameter are prepared using transparent die and pressing machine as explained in section 8.3.2.3. The pictures of pallets are shown in Figure 8.15. We found that 5 and 10 wt% ExG is not sufficient to impregnate PCM inside the ExG matrix, as can be seen from Figure 8.15 (a & b). The higher 15 and 20 wt% ExG based samples showed complete impregnation of eutectic PCM, Figure 8.17 (c & d).

Figure 8.15: Actual photographs of $LiNO_3$-NaCl/ExG composites with 5, 10, 15 and 20 wt% of ExG

The thermal conductivities of prepared samples are measured using Hot Disk TPS 2500S thermal constant analyzer, following the detailed procedure by Kumar et. al. 2017. The measurements are repeated five times and averaged thermal conductivity is plotted in Figure 8.16. The respective errors are shown simultaneously.

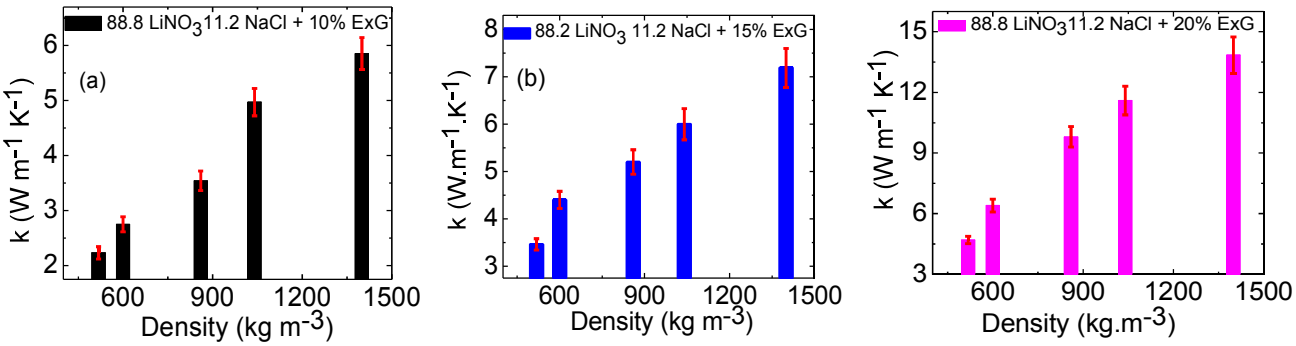

Figure 8.16: Thermal conductivity of $LiNO_3$-NaCl/ExG composites with standard deviations at densities 520, 620, 1000, and 1400 kg m^{-3} with (a) 10% ExG, (b) 15% ExG, and (c) 20 % ExG.

Thermal conductivity of pristine 88.8 wt% $LiNO_3$ - 11.2 wt% NaCl eutectic was 0.82 ± 0.03 W m^{-1} K^{-1}. Further, we observed that the thermal conductivity values are increasing linearly with density, as can be seen in Figure 8.16 for different wt% ExG composite samples. The average thermal conductivities of $LiNO_3$-NaCl/ExG composites at different densities are listed Table 8.3.

Table 8.3: Thermal conductivity of 88 wt% $LiNO_3$ – 11.2wt% NaCl/ ExG composites at different wt% of ExG and densities

Density (kg m^{-3})	Thermal conductivity of LiNO3-NaCl/10% ExG with SD (W m^{-1} K^{-1})	Thermal conductivity of LiNO3-NaCl/15% ExG with SD (W m^{-1} K^{-1})	Thermal conductivity of LiNO3-NaCl/10% ExG with SD (W m^{-1} K^{-1})
520	2.23 (S.D. 0.07)	3.46 (S.D. 0.12)	4.7 (S.D. 0.18)
620	2.75 (S.D. 0.09)	4.4 (S.D. 0.0.18)	6.4(S.D. 0.31)
860	3.54 (S.D. 0.16)	5.2 (S.D. 0.0.26)	9.8(S.D. 0.0.51)
1000	4.97 (S.D. 0.27)	6 (S.D. 0.33)	11.6 (S.D. 0.0.72)
1400	5.85 (S.D. 0.36)	7.19 (S.D. 0.41)	13.84 (S.D. 0.91)

Thermal conductivity of eutectic $LiNO_3$-NaCl was enhanced from 0.82 to 13.84 W m^{-1} K^{-1} for 20 % ExG at 1400 kg m^{-3} PCM-ExG composite density and found maximum among the investigated samples. The density of composite is an important aspect to realize the high thermal conductivity composite systems, as can be inferred from Figure 8.16 that composites with the lowest density ~600 kg m^{-3} is showing low improvement in thermal conductivity and very little enhancement in the thermal conductivity has been observed with increasing ExG wt% in composite system. However, thermal conductivity is enhanced significantly with increasing density for all considered wt% ExG composite samples, where higher weight fraction has shown relatively large enhancement in comparison to that of lower weight fraction ExG.

8.5 CONCLUDING REMARKS

Natural graphite flakes were exfoliated using thermochemical method and about 250 times volume expansion was observed under optimized exfoliation process conditions. The organic PCM-

ExG composites were prepared with simple mixing process. The organic PCM impregnated inside ExG pores using capillary action. 15% ExG was sufficient for shape stabilized PCM-ExG composites. The PCM did not come out side from ExG matrix even under complete PCM melting state. A simple method was developed to prepate high temperature eutectic PCMs using $NaNO_3$, KNO_3, $LiNO_3$ and NaCl at room temperature. Thermal conductivity of PCM-ExG samples was investigated by varying ExG weight fraction and PCM-ExG composites density. We observed that the effect of density on thermal conductivity of PCM-ExG composite is more dominant as compared to that for the mass fraction of ExG. Thermal conductivity enhancement of PCM significantly for thermal energy storage applications.

…